Strain state approximation with Electrical Impedance Tomography using elastoresistive thin-film sensors

Jonas Wagner[1], Christoph Kralovec[1], Daniel Kimpfbeck[1], Herbert Enser[2] and Martin Schagerl[1]

[1] Institute of Structural Lightweight Design, Johannes Kepler University Linz, 4040 Linz, Austria
[2] Institute for Microelectronics and Microsensors, Johannes Kepler University Linz, 4040 Linz, Austria

E-mail: Jonas.Wagner@jku.at

March 2026

Abstract. Electrical Impedance Tomography (EIT) is a method to reconstruct the conductivity or conductivity change inside an area of interest by systematic voltage measurements at the boundaries. Through the use of an elastoresistive thin-film as EIT object, it is possible to draw conclusions about the skin's spatial strain state. This might be utilized for Structural Health Monitoring (SHM) of thin-walled mechanical structures, which are typical for lightweight design. Thereby, the EIT in combination with an elastoresistive thin-film sensor that covers a mechanical structure allows the monitoring of larger areas. The detection and localization of sensor damages and strains is readily state-of-the-art. However, the identification of the 2-dimensional strain state is still an open topic. The present work proposes a model-based method to approximate a homogeneous 2-dimensional strain state by the evaluation of EIT measurements for, (i) electrode movements to find the the major principal strain directions, and (ii) quantitative conductivity changes to find equivalent strain values. The individual element values of a general strain tensor cannot be separated so far, however, for unidirectional strain states this novel evaluation method enables the full identification of the strain tensor. The proposed method is demonstrated and discussed by numerical forward simulations of strain induced sensor deformation and conductivity changes. Subsequently, these results are validated by an experimental study on flat tensile-loaded coupons that are equipped with differently oriented rectangular elastoresistive thin-film sensors each for EIT strain measurements. The proposed method estimates all experimentally tested strain orientations at highest accuracy. Estimation errors and limits of the proposed method are discussed.

Keywords: major principal strain direction, strain state approximation, electrode movements, strain sensor, elastoresistive thin-film sensor, Electrical Impedance Tomography (EIT), Structural Health Monitoring (SHM)

Submitted to: *Smart Mater. Struct.*

1. Introduction

Electrical Impedance Tomography (EIT) is an imaging technique that is used for noninvasive geophysical and medical survey. In the last two decades, the EIT also became popular in the field of Structural Health Monitoring (SHM) of mechanical lightweight structures in, e.g., civil or aircraft engineering. Lightweight design is an optimization process that aims for lowest weight of mechanical components and entire structures while reliably maintaining its functionality. This weight reduction of, e.g., a component on an aircraft, brings additional value by, e.g., fuel savings or increased payload. However, highly optimized mechanical structures suffer from uncertainties of, e.g., manufacturing or operational loading. SHM can reduce these uncertainties. Thus, design margins might be further exploited while extending cost-intensive maintenance intervals. SHM is the continuous and online monitoring of a mechanical structure during operation. It emerged in the 1990s from the conventional Non-Destructive Testing (NDT) which is applied during periodical downtime for maintenance of the structure of interest. Typical NDT methods are visual inspections, ultrasonic testing [1, 2] or x-ray testing [2, 3]. SHM often applies similar methods by means of permanently installed sensor systems. Typical SHM methods apply measurements of ultrasonic waves [4–7] or strains [8, 9].

Recently the EIT is investigated for SHM applications as imaging technique by means of systematic electrical voltage measurements at conductive mechanical components itself or at conductive thin-film coatings. Thereby, in its quality as tomography method, the voltage between attached electrodes is measured at the boundary of an area of interest while excited with known current stimulation paths. The subsequent inverse reconstruction of the EIT problem provides an estimate of the conductivity inside the observed area. This allows conclusions about the conductivity distribution or the conductivity change within the monitored area of interest.

Conductive, i.e., self-sensing, structural materials enable to directly measure structural changes by means of conductivity changes [10–14]. However, metallic structures are highly conductive, and thus, conductivity changes are difficult to measure with today's data acquisition equipment. Carbon fiber reinforced polymers (CFRP), in contrast, provide an adequate conductivity but reconstructions suffer from its high electrical inhomogeneity and anisotropy. In addition, there are materials that are bad conductors and are therefore not suitable for examination by EIT. To overcome these disadvantages, conductive thin-film coatings on the surface of a structure of interest can be used for SHM applications with EIT. Damages in typically thin-walled lightweight structures often rapidly propagate to the surface, and thus, result in thin-film coating cracks that can be easily monitored. The advantage of an elastoresistive thin-film as sensor is that its electrical characteristics can be tailored to the application [15], and furthermore, it can be applied to virtually every substrate material (i.e., it is independent of the material of the structure). For instance, Loyola *et al* [16, 17] investigated the detection of spatial damage by monitoring carbon nanotube based sensor skins using EIT. In addition, further studies deal with the detection of damage using EIT and conductive thin-film coatings on various materials [18–21]. Moreover, Tallman and Smyl [22] provide a good review of the current state of research of EIT in the field of SHM. Furthermore, typical thin-film materials are elastoresistive. This enables to monitor also the spatial strain state of the area of interest [23], and thus, also to reveal damage below the surface (e.g., delamination in composites). Loh *et al* [24] showed in this context the detection of spatial strain and impact damage using sensing skins monitored by EIT. Wagner *et al* [25] utilized the sensor skins elastoresistivity to monitor the sole mechanical loading resulting a single equivalent strain value calculated from the proportional single valued conductivity change. However, these single equivalent strain values do not allow conclusions on the underlying 2-dimensional strain state, i.e., the correlation of the elements of the strain tensor and the equivalent value is unknown. Consequently, default inverse EIT image reconstruction does not allow the full identification of the strain state of a surface. Yokaribas *et al* [26] addressed this issue and presented EIT methodologies to identify multi-axial strain states. These are based on the elastoresistive behavior considering the underlying EIT stimulation pattern (i.e. current flow direction) and the corresponding strain components.

The novel approach presented in this study allows to conclude on the strain state by analyzing the sensor distortion and subsequent electrode displacements under strain. The areal deformation due to the strain changes the electrode distances and causes image reconstruction artifacts. An effect, which is well known in the medical and geophysical fields, where electrode misplacement yields incorrect representation of the underlying model and consequently provides inaccurate results. Therefore, methods were developed to compensate these so-called electrode movements by identifying and including these model inaccuracies in the regularization [27–29].

The present work proposes a novel methodology that uses this electrode displacement identification together with sensor conductivity changes to conclude on the principal strain directions of an observed

uniform 2-dimensional strain field. Both, the determination of the principal strain directions and the reconstruction of a quantitative equivalent strain value are discussed and validated by numerical simulations and physical experiments. The considered case example is a uniaxial tensile test at a plate equipped with an elastoresistive thin-film sensor that is rotated to imitate different principal strain directions.

2. Theory

EIT is an imaging technique using voltage measurements to provide information about the conductivity in a specified area of interest. The fundamental mathematical approach is an elliptic partial differential equation of the form

$$\nabla \cdot (\sigma(\boldsymbol{r})\nabla\phi(\boldsymbol{r})) = 0, \qquad \boldsymbol{r} \in \Omega, \tag{1}$$

the so-called Kirchhoff's law [30, 31]. This states, that for a known conductivity distribution $\sigma(\boldsymbol{r})$ and an applied voltage field $\nabla\phi(\boldsymbol{r})$ in a domain Ω, the summation of current density distribution is zero. This equation can be solved numerically for any domain Ω. In the present work the finite element (FE) method with a complete electrode model (CEM) was selected, resulting in the boundary conditions [32]

$$\phi(\boldsymbol{r}) + z_l\sigma(\boldsymbol{r})\frac{\partial\phi(\boldsymbol{r})}{\partial\boldsymbol{n}} = U_l, \quad \boldsymbol{r} \in e_l, \;\; l = 1, 2, ..., L \tag{2}$$

$$\int_{e_l} \sigma(\boldsymbol{r})\frac{\partial\phi(\boldsymbol{r})}{\partial\boldsymbol{n}}\mathrm{d}S = I_l, \quad \boldsymbol{r} \in e_l, \;\; l = 1, 2, ..., L \tag{3}$$

$$\sigma(\boldsymbol{r})\frac{\partial\phi(\boldsymbol{r})}{\partial\boldsymbol{n}} = 0, \qquad \boldsymbol{r} \in \partial\Omega \setminus \cup_{l=1}^{L} e_l. \tag{4}$$

Thereby, U_l and I_l describe the voltage and current, respectively, at the l-th electrode with the electrode-area e_l. Moreover, $\boldsymbol{n}$ describes the normal vector to the boundary $\partial\Omega$ of the domain Ω.

In general, EIT deals with relating voltages at the attached electrodes to applied current between two electrodes due to the given conductivity inside the domain of interest Ω. Knowing the conductivity inside this domain, the linear system of equations

$$\mathbf{H}\boldsymbol{\sigma} = \boldsymbol{v} \tag{5}$$

can be formulated. This is referred to as the forward problem of EIT, where $\boldsymbol{\sigma}$ represents the isotropic conductivities of the finite elements, $\boldsymbol{v}$ the voltages between the electrodes and $\mathbf{H}$ the sensitivity matrix. In the present work, this forward problem is used to numerically simulate voltage measurements for EIT reconstruction testing.

However, the inverse reconstruction, i.e., the actual EIT problem is given by

$$\hat{\boldsymbol{\sigma}} = \mathbf{R}\boldsymbol{v}. \tag{6}$$

Due to the fact, that the linear system in (5) is overdetermined, a pseudo-inverse matrix is established with $\mathbf{R}$. In this case, it is an ill-posed mathematical problem. To overcome this circumstance, regularization is implemented [30, 31]. In this way, an approximation of the conductivity distribution $\hat{\boldsymbol{\sigma}}$ in the domain Ω is obtained. In addition, differential EIT is used to analyze the change in spatial conductivity. In contrast to the absolute EIT, two voltage measurement sets (one for reference and one for reconstruction of change) are needed to reconstruct the spatial conductivity change. Thereby, the differential EIT allows a more stable reconstruction as it has a lower susceptibility to measurement noise and deviations between the reality and the applied FE sensor model [33, 34].

In order to solve the inverse reconstruction of the difference EIT in (6), a maximum *a posteriori* (MAP) regularization approach is used. For this purpose, the Gauss-Newton one-step algorithm is utilized [35–37]. Thus, for the inverse difference EIT problem, the linearized form of (6) becomes

$$\Delta\hat{\boldsymbol{\sigma}} = \left(\mathbf{H}^\intercal\mathbf{W}\mathbf{H} + \lambda^2\mathbf{Q}\right)^{-1}\left(\mathbf{H}^\intercal\mathbf{W}\right)\Delta\boldsymbol{v}. \tag{7}$$

Thereby, the vector $\Delta\boldsymbol{v}$ denotes the change of voltage at the electrodes and $\Delta\hat{\boldsymbol{\sigma}}$ the estimated conductivity change as result. The matrix $\mathbf{W}$ serves as a weight matrix. Furthermore, the regularization is realized through the hyperparameter λ which controls the influence of the regularization matrix $\mathbf{Q}$.

However, the change in conductivity due to strain can be separated into two parts. The main effect is the elastoresistive behavior of the sensor material. A further effect is, the distortion of the sensor body which changes the positions of the electrodes relative to each other, and thus, the distance between them. This changed electrode distances lead to a change of the measured boundary voltages. Gómez-Laberge and Adler [28], Soleimani *et al* [27] and Boyle *et al* [29] present the following extension of (7), which allows to consider electrode movements in the linearized inverse reconstruction of the spatial conductivity. For this purpose, the regularization is separated into a regularization matrix $\mathbf{Q}_c$ for the conductivity change and a matrix $\mathbf{Q}_m$ for the electrode movement.

$$\mathbf{Q} = \mathbf{Q}_c + \mu^2\mathbf{Q}_m. \tag{8}$$

The model hyperparameter $\mu = \sigma_c/\sigma_m$ defines the tradeoff between conductivity changes and electrode movements. It is based on the *a priori* amplitudes of the conductivity change σ_c and electrode movement σ_m. Assuming the constraint $\lambda = \sigma_n/\sigma_c$, where σ_n describes the measurement noise amplitude, (7) can

be expressed in a linearized and simplified form by [27]

$$\Delta\hat{\boldsymbol{\sigma}} = \left(\mathbf{H}^\intercal\mathbf{W}\mathbf{H} + \frac{1}{\sigma_c^2}\mathbf{Q}_c + \frac{1}{\sigma_m^2}\mathbf{Q}_m\right)^{-1}(\mathbf{H}^\intercal\mathbf{W})\,\Delta\boldsymbol{v}. \tag{9}$$

This allows the inverse reconstruction by EIT to estimate the conductivity change and electrode movements separately. Thus, with this EIT reconstruction data, it is possible to use the electrode movements to approximate the major principal strain direction and the conductivity change to derive an equivalent strain amplitude, as proposed in the present research.

3. Case example

The case example used in the present research is the uniaxial tensile test at a polymeric coupon equipped with a square elastoresistive thin-film sensor. It serves as basis for the simulations as well as the subsequent experimental tests. By changing the sensor orientation, different principal strain directions can be simulated under a homogeneous strain state (cf. figure 1). For the definition of the sensor orientation, the angle α serves as the rotation angle of the sensor and thus, defines the rotation of the local x-y-coordinate system of the sensor with respect to the global X-Y-coordinate system of the test coupon. In addition, the 1-2-coordinate system represents the two principal strain directions. A characteristic of the uniaxial tensile test is that the principal strain directions are equal to the coordinate system of the test coupon. The orientation of the principal strain directions to the x-y-coordinate system of the sensor is given by the rotation angle θ. Consequently, for the uniaxial tensile test $\theta = \alpha$ applies.

For validation of the simulation results, physical experiments are conducted. Therefore, carbon black-based silkscreen printed elastoresistive thin-film sensors with 16 electrodes made of silver conductive epoxy resin and silver conductive paste are used. These have already been tested and deemed suitable for EIT-based reconstructions of strain [25, 38] (cf. figure 2). The present sensor production is not sophisticated enough to ensure uniform sensor properties such as the conductivity in the unstrained state. Therefore, the Montgomery method [39,40] is used to control the EIT results (cf. [38]). The Montgomery method requires a thin rectangular shape of the analyzed conductive body and electrodes at its four corners. Consequently, the thin-film sensor shape is quadratic. The side length of the sensor is 30 mm. A coupon made of poly(methyl methacrylate) (PMMA) with the dimensions 160 mm × 48 mm × 8 mm serves as the tensile specimen.

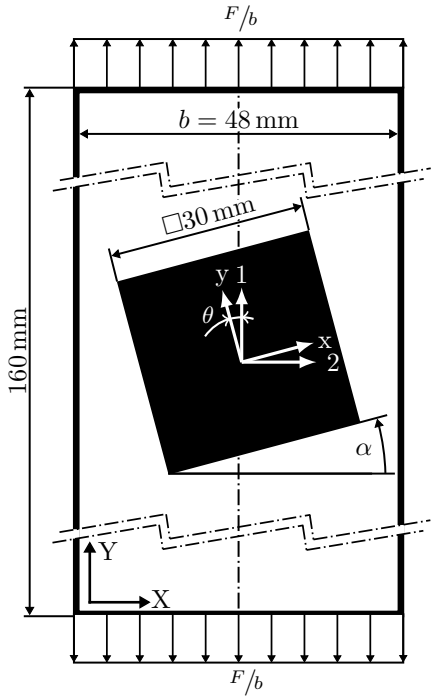

Figure 1. Schematic setup of the uniaxial tensile experiment with the sensor applied to a test coupon and rotated by α, including the associated coordinate systems.

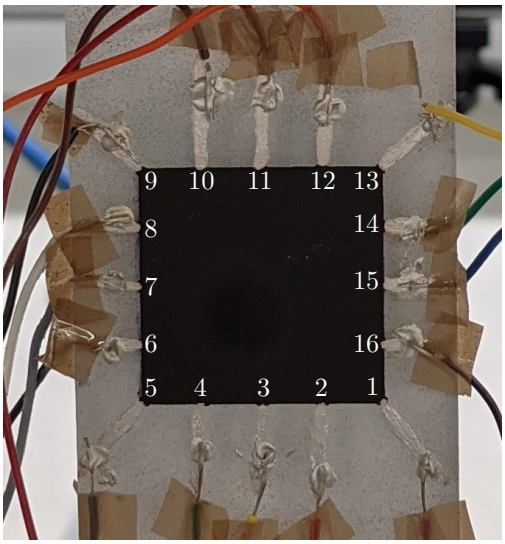

Figure 2. Elastoresistive thin-film sensor made of carbon black with 16 numbered electrodes applied on a coupon made of PMMA with an angle $\alpha = 0°$.

3.1. EIT parameter selection

In order to perform the inverse reconstruction of the conductivity change $\Delta\sigma$ under consideration of the electrode displacement by EIT, the parameters σ_c and σ_m of (9), have to be defined. This parameter selection is based on a definition described

by Soleimani *et al* [27]. Therefore, the model hyperparameter $\mu = \sigma_c/\sigma_m$, which represents the relationship between the conductivity changes and the electrode movements (which result from the strain), must be determined. Foregoing experiments with the utilized sensor material indicate that for a sensor base conductivity σ_0 of approximately 1 500 S/m, a conductivity change $|\Delta\sigma|$ in the range of 10 S/m follows for a unidirectional strain ε_{YY} of 1 000 µm/m that is homogeneous over the whole sensor area. Therefore, the model hyperparameter μ can be calculated according to Soleimani *et al* [27] by

$$\mu = \frac{\Delta\sigma/\sigma_0}{\varepsilon} \approx 6.\overline{6}\,. \tag{10}$$

The choice of the regularization parameter λ is based on a heuristic selection made on the basis of inverse EIT simulations. The Laplace prior is utilized for solving the inverse problem of EIT. This provides a the conductivity change of the sensor in the following research.

3.2. Data Acquisition

As stated in the theory section, the difference EIT is used in this work. This means that two sets of electrode voltage measurements are required under two different loading states. Such voltage measurement sets are specified by the stimulation pattern (also referred to as current injection pattern), which determines the sequence in which the current is injected and the voltage is measured at the electrodes. For this research the opposite pattern [13, 25] is used. Thereby, the first current path passes from electrode 1 to electrode 13 (cf. figure 2 for electrode numbers), the second current path from electrode 2 to electrode 12, and so on. Thus, for the type of electrode layout used and by omitting the voltage measurements at the current-carrying electrodes, 120 voltage measurement values are obtained, representing one voltage measurement set. For the acquisition of this voltage data, a switch developed by Gschoßmann *et al* [41] is used in combination with a *Keithley 6220* current source and two *HBM QuantumX MX840B* voltmeters. A more detailed description of the measurement setup is further given by Wagner *et al* [25].

4. Simulation-based methodology

In the following section, the methodology for approximating the strain state is presented. It is shown, that the major principal strain direction and conductivity change can be approximated using inverse EIT reconstruction. Thereby, the voltage measurement data sets required for the inverse EIT reconstruction are obtained by solving the forward problem. Subsequently, the presented methodology is tested in detail and its limitations are discussed.

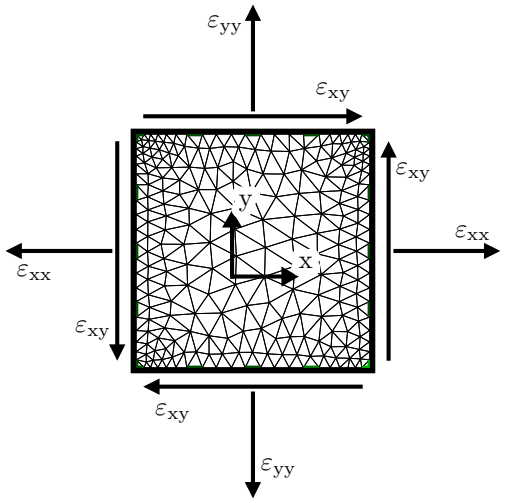

Figure 3. 2-dimensional EIT sensor FE model with simplified mesh and the three independent elements of the 2-dimensional strain tensor for the x-y-coordinate system.

4.1. Simulation

Simulations are performed using MATLAB® in combination with the open source software EIDORS [42]. The used FE simulation model of the thin and planar sensor is represented in figure 3. The considered homogeneous 2-dimensional strain state is defined by ε_{xx}, ε_{yy} and ε_{xy} (with respect to the x-y-coordinate system given in figure 1). The EIT reconstruction is governed by a linear system of equations, thus, strain state reconstruction can be investigated independently for every tensor element. Therefore, the proposed method is numerically tested by applying normal strains ε_{xx} and ε_{yy} and shear strain ε_{xy} resulting from tensile and compressive loading and shear loading, respectively, alone and combined. The considered strain states are simulated by mesh distortion. As demonstrated by Zhao *et al* [20] for carbon nanotube sensor material, the change in conductivity may not be linear and generally depends on the entire strain state. For the carbon black sensor material used in the present work no elastoresistivity (strain-conductivity correlation) is documented but based on experiments already conducted by Wagner *et al* [38] similar behavior may be expected. In the simulations the elastoresistive behavior (relation of normal strain ε to conductivity change $\Delta\sigma$) is assumed to be linear and only related to the dominant strain ε_1 or ε_2 (an assumption that approximates the experimental behavior well, cf. figure 15: linearized elastoresistivity coupon$_1$ and coupon$_3$). Based on the experiments performed in this research, a strain of

$\varepsilon_{YY} = 1000\,\mu m/m$ results in a conductivity change of $\Delta\sigma = -10\,S/m$, which is used for simulation.

4.2. EIT reconstruction results

At the beginning, electrode potential changes due to homogeneous normal and shear strain states are simulated. These load states are simulated without and with lateral strain (i.e. Poisson's ratio $\nu = 0$ and $\nu = 0.35$). The EIT reconstruction results of the simulations are shown in figure 4. The arrows at the electrodes represent the approximation of the normalized electrode displacement, reconstructed from the voltage potential changes simulated by the distorted FE sensor model. The color shading indicates the reconstructed conductivity change, which results from the simulated sensor strain. The different considered load cases can readily be identified visually from the indicated electrode movements. Furthermore, it is noticeable that despite not simulating lateral strains ($\nu = 0$), such electrode movements due to lateral strain are visible in the reconstructed results (cf. figure 4.a and 4.c). Additionally, simulations with lateral strain ($\nu = 0.35$) result in electrode movement vectors with similar vector length (cf. figure 4.b and 4.d). This results from the algorithm used (algorithm implemented in EIDORS [42]) to reconstruct the electrode movements, which returns an approximation of electrode movement directions but only a unit length for their displacement magnitudes (cf. section 4.4). Thus, by sole application of this electrode movement reconstruction algorithm, the major principal strain direction may be approximated but conclusions on the dominating strain are not possible, i.e. it is not possible to differentiate whether tension or perpendicular pressure loading is dominant (compare results in figure 4.a with 90° rotated results in figure 4.c and results in figure 4.b with rotated results in figure 4.d, respectively). However, this drawback can be addressed by evaluation of the elastoresistive behavior of the sensor, which allows to monitor the homogeneous spatial conductivity change. The conductivity change direction allows to differ between a tensile and a pressure dominated load state. In order to obtain more realistic simulation data for the further investigation, additionally lateral strain is considered by the specified sensor mesh distortions. Due to the PMMA coupons used, a Poisson's ratio of $\nu = 0.35$ is assumed for the further simulations. This Poisson's ratio is derived from experimental measurements using the digital image correlation system (DIC; cf. Section 5). Figure 5 shows simulated EIT image reconstruction results including the electrode movement with different rotation angle α of the applied sensor (cf. figure 1). A visual recognition of the angle of the major principal strain direction

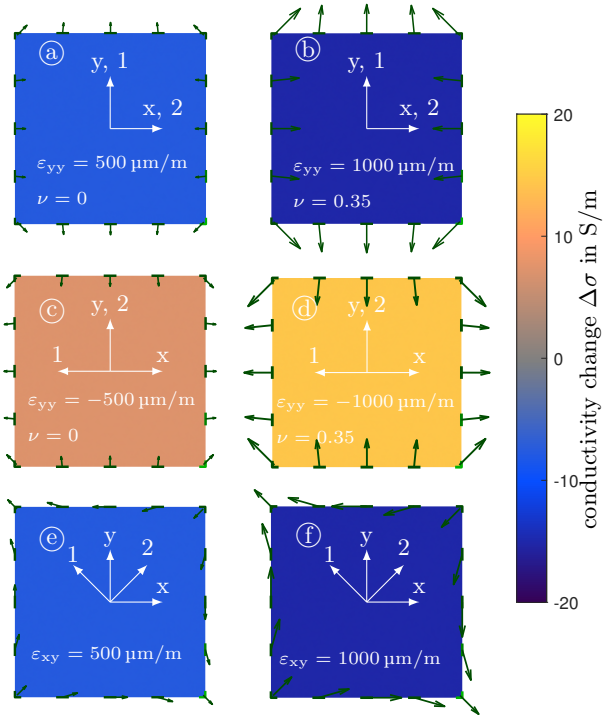

Figure 4. Conductivity change (color shading) and electrode movement (indicated by arrows) EIT reconstruction results for simulation data (without and with lateral strain) of pure tensile (a, b), pressure (c, d) and shear (e, f) strain. x – y denotes the sensors coordinate system and 1-2 are the reconstructed major and minor principal strain directions

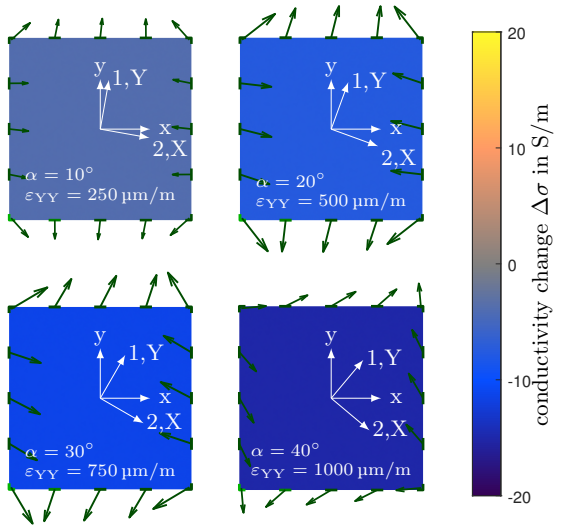

Figure 5. Conductivity change (color shading) and electrode movement (indicated by arrows) EIT reconstruction results for simulation data of a uniaxial tensile test at different strains and load angles α. x-y denotes the sensors coordinate system and 1-2 are the reconstructed major and minor principal strain directions

from the reconstructed electrode displacements is not possible and not suitable. Therefore, a method for the evaluation of the major principal strain direction

from the electrode movements of the inverse EIT reconstruction is presented in the following section.

4.3. Identification of the major principal strain direction

The major and minor principal strain directions (1-2) are described by the rotation angle θ with respect to the sensor coordinate system (x-y-coordinate system; cf. figure 1). Thereby, the major principal strain direction θ is to be approximated from electrode movements obtained by the inverse EIT. It is found that for any major principal strain direction $-90° \geq \theta \geq 90°$, each electrode movement vector has a unique angle γ_i. Thereby, only half the angular range is relevant due the symmetrical plane strain tensor. For demonstration purposes, figure 6 shows the electrode movement angles γ_1 and γ_9 at the respective electrode with a simulated sensor angle rotation $\alpha = 0°$.

Consequently, the relation between the electrode movement angle γ_i and the major principal strain direction θ must be determined. This can be overcome through the forward solution and the subsequent inverse reconstruction of the EIT problem. Simulating the distortion of the sensor shape as a function of the sensor rotation angle α allows the electrode voltages to be derived as a result of the loading angle. From these simulated electrode voltages, the associated electrode movements can be reconstructed by EIT (cf. section 2). Plotting the individual electrode movement angles γ_i over the underlying simulated principal strain direction θ (of a unidirectional load) gives a unique and load magnitude independent relationship for each electrode. Thus, the major principal strain direction θ can be approximated by the movement of every single electrode movement angle γ_i. Figure 7 displays the found relationships between the reconstructed electrode movement angles γ_i and the simulated major principal strain directions θ. One can also refer to this as an angular transformation. A lookup table is created to allow rapid calculation of the major principal strain direction θ as a function of the respective electrode motion angle γ_i. For this purpose and due to symmetry properties, the forward EIT simulation and the inverse EIT reconstruction are solved stepwise between $-90° \geq \theta \geq 90°$. In the further steps, this angular transformation data set is used to find an approximation of the major principal strain direction θ. It is important to note that the angular transformation data set is tailored to the sensor model (sensor shape, electrical properties and electrode positions) and must be re-determined for changing parameters.

Since electrode movements are given for all electrodes i, an equal number of independent major principal strain direction approximations θ_i can be obtained. To overcome measurement uncertainties, such as measurement noise, the approximated major principal strain direction θ is determined by the circular mean from all available major principle strain directions θ_i (16 due to the used sensor model). Combining the major principal strain direction θ with the strain amplitude due to the conductivity change $\Delta\sigma$, the strain state is fully approximated for the simple case of a uniaxial strain state.

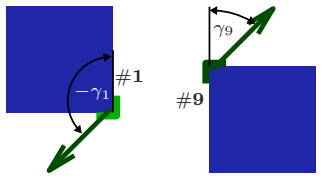

Figure 6. Illustration of the reconstructed electrode movement angles γ_1 and γ_9 at the electrodes 1 and 9 at a load angle α of 0°.

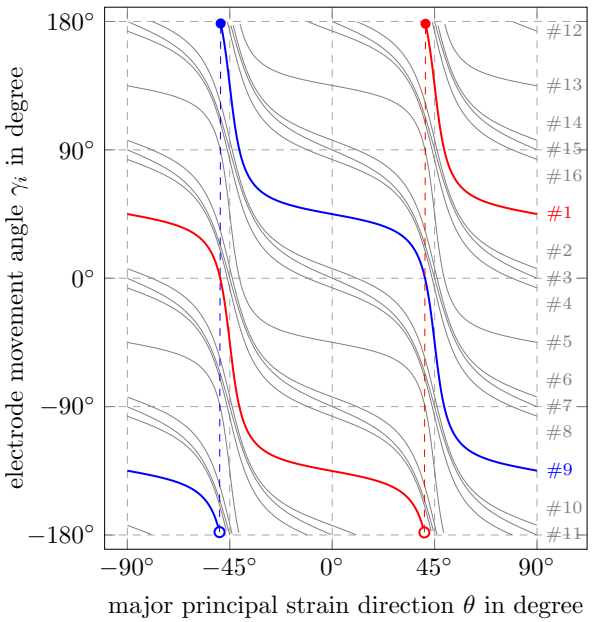

Figure 7. Angular transformation between the major principal strain direction θ and the EIT related electrode movement angles γ_i including the highlighted γ_1 and γ_9 illustrated in figure 6.

4.4. Limitations

The testing of the algorithm is done with two independent studies. First, its robustness to measurement noise is tested. This is done by adding white noise to the simulated measurement data to artificially generate a signal-to-noise-ratio (SNR) of 60 dB, 70 dB and 80 dB (SNR found in the experimental investigation is approximately 75 dB). In total, a number of $N = 10\,000$ simulations with a random sensor rotation angle α between $-45° \geq \alpha \geq 45°$ is used (homogeneous uniaxial strain-states with

a Poisson's ratio $\nu = 0.35$). Figure 8 shows the approximated major principal strain directions θ over the simulated true values α and their approximation errors for the different considered SNR in box plots. Thus, for the experimental EIT data (SNR $\approx 75\,\mathrm{dB}$) a good reconstruction can be expected. Below a SNR of 60 dB, the reconstruction of the load angle becomes significantly less accurate. However, this is a comparatively low SNR, also for experimental measurements, and thus, considered uncritical.

The second study addresses the methods limitation to strain states that are not uniaxial. Therefore, electrode potential changes are simulated for different strain ratios $\frac{\varepsilon_{xx}}{\varepsilon_{yy}}$ ($\varepsilon_{xy} = 0$) at an unrotated sensor ($\alpha = 0°$). Figure 9 shows the reconstructed major principal strain direction θ for a simulated strain ratio between $-2 \geq \frac{\varepsilon_{xx}}{\varepsilon_{yy}} \geq 2$. The discontinuity at $\frac{\varepsilon_{xx}}{\varepsilon_{yy}} = 1$ is striking. The discontinuity occurs because at this point the major principal strain direction changes from the y-axis to the x-axis ($\varepsilon_{xx} > \varepsilon_{yy}$) or vice versa. Furthermore, when $\frac{\varepsilon_{xx}}{\varepsilon_{yy}} = 1$, no unique major principal strain direction can be determined because in this particular case the strain is equal in both directions. However, for the major principal strain approximations without noise the method works perfect for the simulated strains. If noise is present, the performance is increasingly reduced. Nevertheless, the approximation remains good for realistic SNR levels and some distance to $\frac{\varepsilon_{xx}}{\varepsilon_{yy}} = 1$. Towards the strain ratio $\frac{\varepsilon_{xx}}{\varepsilon_{yy}} = 1$ the approximation is increasingly corrupted. However, this can be explained due to the change of the major principal strain direction from $\sigma_1 = \varepsilon_{yy}$ to $\sigma_1 = \varepsilon_{xx}$ for $\frac{\varepsilon_{xx}}{\varepsilon_{yy}} > 1$ Thus, the proposed method for the approximation of the principal strain direction can be assumed as very robust over a wide range of strain states, and in particular, for strain states with a very dominant principal strain direction (as considered for experimental validation).

5. Experimental validation

The experimental validation of the proposed strain state approximation approach is done by means of uniaxial tensile loaded coupons with differently rotated elastoresistive thin-film sensors (cf. section 3). For investigation the sensor rotation angles $\alpha = 0°, 15°, 30°$ and 45° are considered, thus, providing experimental EIT measurements of homogeneous strongly tensile dominated strain states with the same principal strain direction (cf. figure 1). Figure 10 shows the four test coupons used including the silkscreen printed sensors.

These coupons are tensile loaded in two consecutive cycles (displacement controlled with 200 µm/s) with 9 loading stops of 70 seconds (with 60 seconds pause before measurement to mitigate material effects)

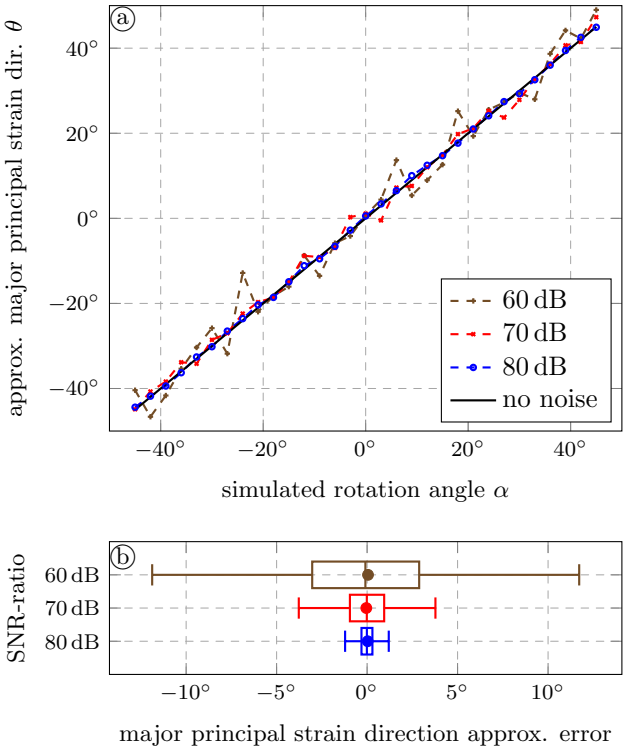

Figure 8. a) Approximated major principal strain direction θ over $N = 10\,000$ randomly simulated rotation angle $-45° \geq \alpha \geq 45°$ for different SNR. b) Box plots of approximation errors $e = \theta - \alpha$ for $N = 10\,000$ simulations ($-45° \geq \alpha \geq 45°$) and for different SNR.

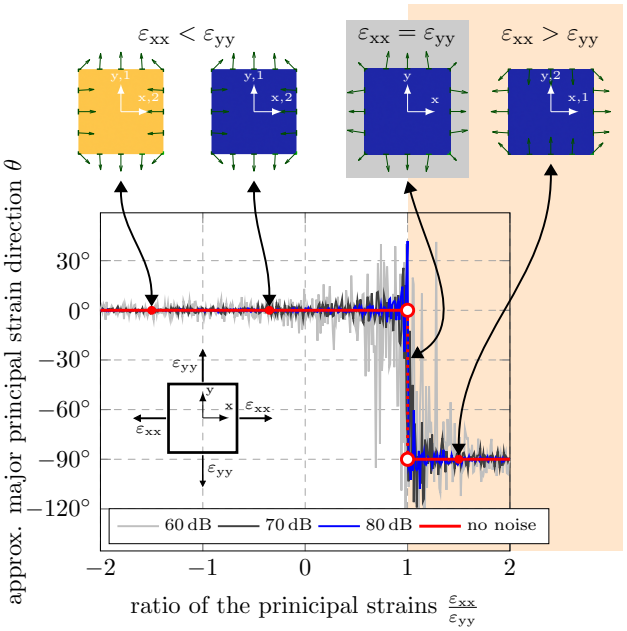

Figure 9. Reconstructed major principal strain direction θ_r at strain ratios between $-2 \geq \frac{\varepsilon_{xx}}{\varepsilon_{yy}} \geq 2$ with an simulated load angle $\alpha = 0°$ and different signal-to-noise ratios.

to allow voltage measurements for EIT in different static loading conditions. In this context, the strain-time curve of figure 13.a displays the two tensile load cycles with the 9 EIT reconstruction load levels, applied to every coupon. For verification of the intended homogeneous tensile loading, the the strain on the back of the coupons is monitored by using a digital image correlation system (DIC). Figure 11 shows a photographic image of the experimental setup, consisting of the clamped coupon with a rotated sensor applied ($\alpha = 30°$) and DIC cameras in the background. The view of the DIC cameras (cf. figure 11) including the evaluation of the strain state at an arbitrary load is shown in figure 12, confirming the intended strain state to be very homogeneous over the entire sensor area.

The results of the EIT-based approximation of the major principal strain directions for all measured load levels are presented in figure 13.b. The correlation between true (given by sensor rotation α) and reconstructed major principal strain direction θ is very well over all considered load levels. Deviations between load cycle one an two are expected to result from residual strain in the PMMA test coupons, set-in-effect of the elastoresistive thin-film sensor behavior [43] and measurement noise. Divergent behavior of reconstruction results for different principal strain directions can be assigned to slight differences between the sensors that are applied to the the four coupons.

Moreover, the EIT-based approximation of the principal direction of the principal strain directions works better at higher strains, which makes sense as relative measurement errors become smaller. Nevertheless also for small strains the approximation error remains below 5° for all considered coupons and sensor rotation angles, respectively. In some cases, an offset is also evident. This may be due to insufficiently accurate EIT models or an inaccurate EIT reconstruction parameter selection. Another reason could be a slightly tilted clamping of the coupon in the tensile test (i.e. rotation of the coupon around the global Z-axis). For the reconstruction of the experimental measurement data, the same EIT reconstruction parameters were used as for the reconstruction of the simulated voltage measurement data. Figure 14 shows underlying EIT conductivity and electrode movement/displacement image reconstruction results of the four considered test specimens at different load levels. A scattering of the reconstructed electrode movements compared to the simulation data without noise (cf. figure 5) is evident. Nevertheless, a good approximation of the major principal strain direction θ is possible. Note that the length of the electrode movement arrows is not related to the strain magnitude, since different sensors are used and therefore different scaling is applied.

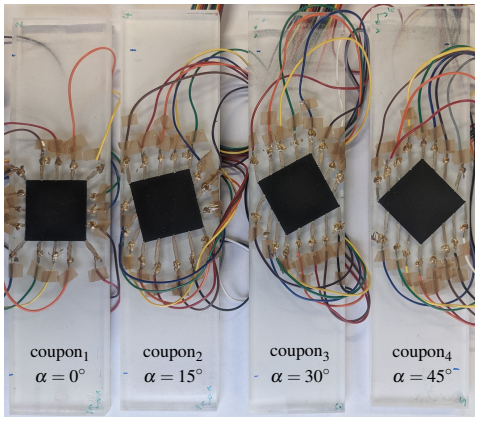

Figure 10. Tensile test coupons with rotated elastoresistive sensors

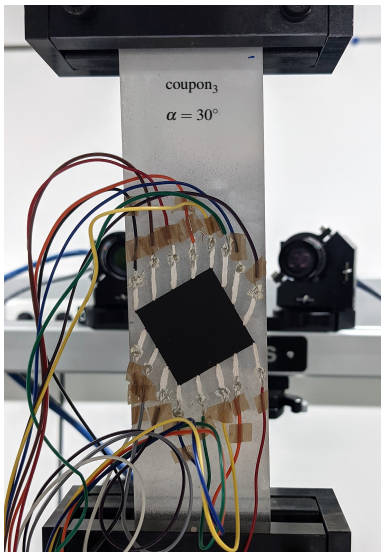

Figure 11. Experimental setup showing clamped tensile test coupon$_3$ with a sensor rotation angle $\alpha = 30°$ and with the DIC cameras in the background

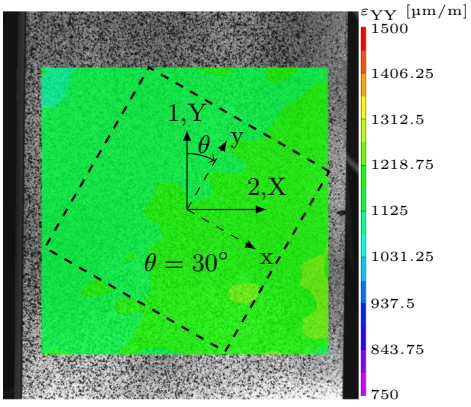

Figure 12. Rear view of tensile test coupon$_3$ (also shown in figure 10 and figure 11) with DIC strain analysis under 100% load (cf. figure 13).

For better illustration and visibility of the electrode movement arrows, the length is normalized.

In addition, an approximately linear relation between strain and sensor conductivity change is observed. Figure 15 shows the exemplary EIT conductivity reconstruction results over the coupon's measured strain ε_{YY} for the cyclic tensile test of coupon$_3$ ($\alpha = 30°$). This fits with the assumptions chosen in section 4.1 (the elastoresistive behavior is assumed to be linear and governed by the dominant strain ε_1 or ε_2). Thereby, the four sensors show a similar elastoresistivity with small deviation of the unstrained conductivity probably caused by differences in thickness of the sensor material (see linearized elastoresistivity of coupons 1 and 3 in figure 15). It follows that for a uniaxial load state and known material parameters (Poisson's ratio), the quantitative strain amplitude can be calculated from the reconstructed conductivity change and the linearized elastoresistivity (known material property). Consequently, the strain state can be fully approximated by the proposed approach.

6. Conclusions

The present research proposes and experimentally demonstrates a novel method to approximate a homogeneous 2-dimensional strain state by EIT-based conductivity and electrode movement reconstruction at elastoresistive thin-film sensors. As case example a uniaxial tensile test is utilized. Thus, a homogeneous static strain state is considered. In order to alter the major principal strain direction, differently oriented sensors are investigated. Several tensile coupons with rotated sensors were presented for this purpose. This experimental framework is to be evaluated by simulations and experiments. In doing so, a novel methodology to approximate the strain state based on EIT reconstructions is proposed.

The proposed approach uses EIT-based equivalent strain value reconstruction in combination with a novel method to identify the major principal strain direction. The latter bases on the EIT reconstruction of electrode movements and is investigated in the present work by means of numerical simulations and physical experiments. Electrode movements inevitably occur when the sensor is subjected to strain and thus becomes distorted. Thereby, the major principal strain direction monitoring is load amplitude independent and the strain state of the sensor is monitored simultaneously. The combination of these two allows the approximation of the strain state. An open-source inverse EIT reconstruction algorithm embedded in the evaluation software EIDORS is adapted and used to reconstructed the EIT image results. These results

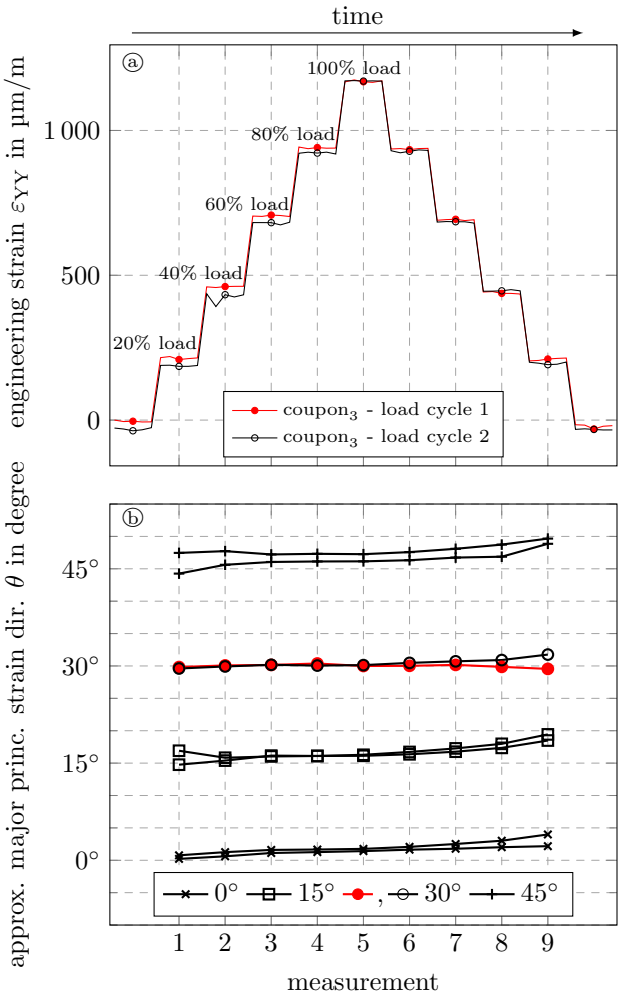

Figure 13. a) Mean axial engineering strain ε_{YY} of two consecutive load cycles with coupon$_3$ ($\alpha = 30$) measured with DIC b) EIT reconstructed major principal strain directions θ from experimental data at nine strain levels over two loading cycles, evaluated for the four tensile test coupons with its four different sensor rotation angles $\alpha = 0°, 15°, 30°$ and $45°$.

including the electrode movements are then processed to determine the major principal strain direction and strain-conductivity change-relation. Therefore, a methodology for obtaining the major principal strain direction using an angular transformation is introduced and presented by means of numerical simulations of EIT measurements. Furthermore, limitations and robustness of the evaluation algorithm are discussed based on simulations with different strain relations and artificial measurement noise levels. Results show a wide and robust applicability of the proposed major principal strain direction approximation method. The full identification of a 2-dimensional strain state (i.e., the numerical identification of all strain tensor elements) is limited to unidirectional strain states. However, an equivalent strain value can be evaluated

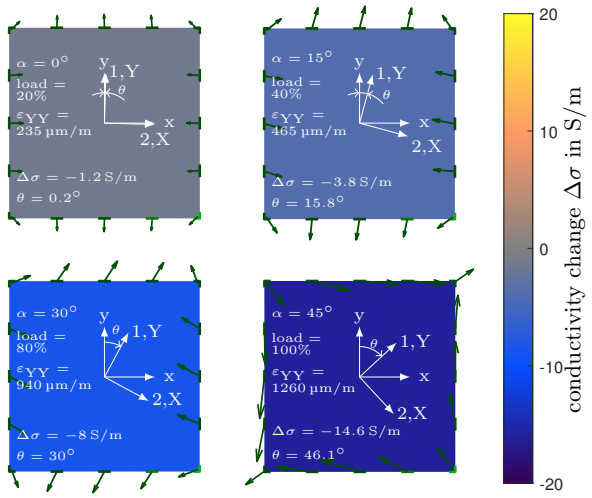

Figure 14. Conductivity change (color shading) and electrode movement (indicated by arrows) EIT reconstruction results from experimental data at different loads and sensor rotation angles α including the approximated major principal strain direction θ.

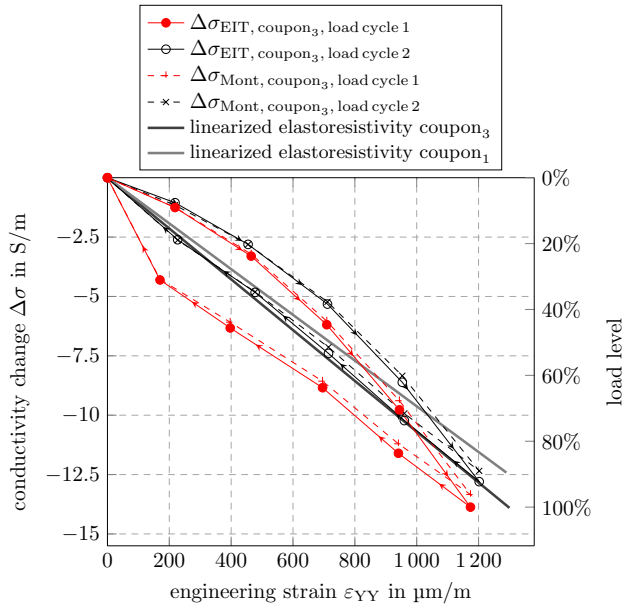

Figure 15. EIT reconstructed and Montgomery Method measured conductivity change $\Delta\sigma$ as a function of the tensile strain ε_{YY} of the coupon with a sensor rotation angle $\alpha = 30°$ and the corresponding load levels of coupon$_3$ including the linearized elastoresistivity of coupon$_3$ and coupon$_1$.

for every strain state. Finally, the proposed algorithm is experimentally demonstrated by uniaxial tensile tests. Therefore, different major principal strain directions were considered by applying rotated sensors to uniaxial tensile test coupons. Results show load independent high accuracy for the reconstruction of the major principal strain directions. Furthermore, the full strain state can be properly reconstructed by assuming linear elastoresistivity.

Future research will address the extension of the proposed method to the full identification of arbitrary 2-dimensional strain states. Therefore, the electrode movement reconstruction algorithm of EIDORS shall be studied and adapted to enable the approximation of the single electrode movements without normalization. Thus, providing a better reconstruction of the true sensor in-plane distortion and strain state consequently. As discussed earlier, the reconstruction algorithm cannot accurately calculate the electrode movements. Instead, it provides an approximation. An improvement for the future would be to adapt the EIT solution approach for calculating the electrode motions to the isotropic material behavior. It would have to be investigated whether, e.g., lateral contractions (lateral strain) can also be mapped correctly with such an approach. Another issue in this work is the use of different sensors. Although these go through the same production steps, they have varying parameters (e.g. conductivity).

[1] Scarponi C and Briotti G 2000 *Composites Part B: Engineering* **31** 237–243 ISSN 1359-8368
[2] Schabowicz K 2019 *Materials (Basel, Switzerland)* **12** 3237 ISSN 1996-1944 31623301[pmid]
[3] Tan K, Watanabe N and Iwahori Y 2011 *Composites Part B: Engineering* **42** 874–884 ISSN 1359-8368
[4] Gorman M R 2009 *Acoustic Emission* (John Wiley & Sons, Ltd) ISBN 9780470061626
[5] Zagrai A N and Giurgiutiu V 2001 *Journal of Intelligent Material Systems and Structures* **12** 709–718
[6] Winklberger M, Kralovec C, Humer C, Heftberger P and Schagerl M 2021 *Sensors* **21** ISSN 1424-8220
[7] Humer C, Höll S, Kralovec C and Schagerl M 2022 *Sensors* **22** ISSN 1424-8220
[8] Katsikeros C and Labeas G 2009 *Mechanical Systems and Signal Processing* **23** 372–383 ISSN 0888-3270
[9] Bergmayr T, Winklberger M, Kralovec C and Schagerl M 2021 *Engineering Failure Analysis* **126** 105454 ISSN 1350-6307
[10] Haingartner M, Gschoßmann S, Cichocki M and Schagerl M 2021 *Structural Health Monitoring*
[11] Koo G and Tallman T 2020 *Composites Part B: Engineering* **190** 107907 ISSN 1359-8368
[12] Hassan H and Tallman T N 2020 *Structural Health Monitoring* **19** 765–780
[13] Nonn S, Schagerl M, Zhao Y, Gschossmann S and Kralovec C 2018 *Composites Science and Technology* **160** 231 – 236 ISSN 0266-3538
[14] Tallman T, Gungor S, Koo G and Bakis C 2017 *Journal of Intelligent Material Systems and Structures* **28** 2617–2629
[15] Kimpfbeck D, Gschoßmann S, Wagner J and Schagerl M 2019 Optimizing the electrical conductivity of cnt embedded thin films printed with industrial inkjet technology for strain sensing applications *Smarte Strukturen und Systeme: Tagungsband des 4SMARTS-Symposiums, 22.–23. Mai 2019, Darmstadt* ed Wiedemann M and Melz (Hrsg) T (Shaker Verlag) pp 339–350
[16] Loyola B R, Saponara V L, Loh K J, Briggs T M, O'Bryan G and Skinner J L 2013 *IEEE Sensors Journal* **13** 2357–2367
[17] Loyola B, Arronche L, LaFord M, La Saponara V and Loh K 2013 Evaluation of the damage detection characteristics of electrical impedance tomography vol 2
[18] Seppänen A, Hallaji M and Pour-Ghaz M 2014 Electrical

impedance tomography-based sensing skin for detection of damage in concrete *Proceedings of the 11th European conference on non-destructive testing (ECNDT 2014), Prague, Czech Republic* pp 6–10
[19] Seppänen A, Hallaji M and Pour-Ghaz M 2017 *Structural Health Monitoring* **16** 215–224
[20] Zhao Y, Gschossmann S, Schagerl M, Gruener P and Kralovec C 2018 *Smart Materials and Structures* **27** 105009
[21] Zhao Y, Schagerl M, Gschossmann S and Kralovec C 2019 *Structural Health Monitoring* **18** 1479–1490
[22] Tallman T and Smyl D 2020 *Smart Materials and Structures* **29**
[23] Wagner J, Kralovec C and Schagerl M 2022 *Materials Today: Proceedings* **62** 2440–2445 ISSN 2214-7853 37th Danubia Adria Symposium on Advances in Experimental Mechanics
[24] Loh K J, Hou T C, Lynch J P and Kotov N A 2009 *Journal of Nondestructive Evaluation* **28** 9–25
[25] Wagner J, Gschoßmann S and Schagerl M 2021 *IEEE Sensors Journal* **21** 5798–5808
[26] Yokaribas V, Kraemer P, Mende A B, Ruhkopf J, Lemme M C and Fritzen C P 2021 *Small Science* **n/a** 2100088
[27] Soleimani M, Gómez-Laberge C and Adler A 2006 *Physiological measurement* **27** S103–13
[28] Gómez-Laberge C and Adler A 2008 *Physiological measurement* **29** S89–99
[29] Boyle A, Crabb M, Jehl M, Lionheart W and Adler A 2017 *Physiological measurement* **38**
[30] Kaufmann S 2015 *Instrumentierung der Bioimpedanzmessung: Optimierung mit Fokus auf die Elektroimpedanztomographie (EIT)* Aktuelle Forschung Medizintechnik – Latest Research in Medical Engineering (Springer Fachmedien Wiesbaden) ISBN 9783658097714
[31] Holder D S 2004 Part 1 of electrical impedance tomography: Methods, history and applications *Electrical Impedance Tomography: Methods, History and Applications* Series in Medical Physics and Biomedical Engineering (Taylor & Francis) pp 3–64
[32] Vauhkonen M 1997 *Kuopio University Publications C. Natural and Environmental Sciences* 110 ISSN 1235-0486
[33] Graham B M and Adler A 2006 *Physiological Measurement* **27** S65–S79
[34] Lionheart W R B 2004 *Physiological Measurement* **25** 125–142
[35] Adler A and Guardo R 1996 *IEEE Transactions on Medical Imaging* **15** 170–179
[36] Adler A, Dai T and Lionheart W 2007 *Physiological measurement* **28** S1–11
[37] Cheney M, Isaacson D, Newell J C, Simske S and Goble J 1990 *International Journal of Imaging Systems and Technology* **2** 66–75
[38] Wagner J, Kralovec C, Kimpfbeck D, Heinzlmeier L and Schagerl M 2023 Framework for strain measurements at cyclic loaded structures with planar elastoresistive sensors applying electrical impedance tomography *European Workshop on Structural Health Monitoring* ed Rizzo P and Milazzo A (Cham: Springer International Publishing) pp 805–815 ISBN 978-3-031-07254-3
[39] Montgomery H C 1971 *Journal of Applied Physics* **42** 2971–2975
[40] dos Santos C A M, de Campos A, da Luz M S, White B D, Neumeier J J, de Lima B S and Shigue C Y 2011 *Journal of Applied Physics* **110** 083703
[41] Gschoßmann S, Zhao Y and Schagerl M 2016 Development of data acquisition devices for electrical impedance tomography of composite materials *Proceedings of the 17th European Conference on Composite Materials ECCM17* ISBN 978-3-00-053387-7
[42] Adler A and Lionheart W R B 2006 *Physiol Meas* 25
[43] Enser H, Sell J K, Hilber W and Jakoby B 2018 *Sensors and Actuators A: Physical* **281** 258–263 ISSN 0924-4247